Astronomical and Astrophysical Transactions (*AApTr*), 2021, Vol. 32, Issue 4, pp. 305–330,
ISSN 1055-6796, Photocopying permitted by license only, ©Cambridge Scientific Publishers

Large-scale magnetic field of the Sun: Evolution of ideas

V.N. Obridko[1,2,*]

[1] *Institute of Terrestrial Magnetism, Ionosphere, and Radio Wave Propagation, Russian Academy of Sciences, Kaluzhskoe Shosse 4, Moscow, 108840, Russia*
[2] *Institute of Continuous Media Mechanics, Ural Branch, Russian Academy of Sciences, Academician Korolev Street 1, Perm, 614013, Russia*

Received 25 November, 2021

In this paper, we discuss the evolution of the concept of the large-scale solar magnetic field. The priority of the large-scale field was established about 60 years ago, when it became clear that the spatial structure and evolution of the solar activity obey certain large-scale laws. The analogy between coronal holes and sunspots and the formation of global complexes of activity are discussed. A technique is presented for a quantitative analysis of the large-scale field over long time intervals based on the hypothesis of potential field in the chromosphere and corona. The concept of the global magnetic-field indices is introduced, and their relationship with other heliogeophysical indices is shown. A negative correlation has been found between the magnitude of the magnetic field and the angular rotation rate of the Sun.

Keywords: Solar activity, global magnetic field

1 Introduction

This issue is dedicated to the joint anniversary of the Astronomical Society and of our journal, Astronomical and Astrophysical Transactions, and it is quite suitable to review the more than 50 year period of investigation of solar magnetic fields at IZMIRAN.

This is a very important problem. The large-scale magnetic fields are a kind of a primary agent that determines the evolution of all magnetic fields in the Sun, including the local ones. For a long time this question raised serious doubts and was hotly debated. It seemed strange from the energy point of view, because the fields that form the large-scale magnetic structure are much weaker than the local fields. In fact, this is a false impression, since the flux of the large-scale magnetic fields distributed all over the solar surface is actually comparable to the flux of the local magnetic fields,

*Email: obridko@izmiran.ru

which are 1000 times stronger. The local fields are rather shallow and, most likely, are located immediately under the photosphere, while the large-scale fields seem to penetrate the entire convection zone; therefore, their contribution is comparable as concerns the mean energy.

The role of the large-scale fields is confirmed by the models of generation of solar and stellar magnetic fields. As follows from all available models, the differential rotation primarily generates a large-scale field (the so-called Ω-dynamo), which subsequently determines the structure and dynamics of the local fields.

This gave rise to the concept of the priority of large-scale and global magnetic fields, which was developed over the past decades with an active participation of IZMIRAN research teams.

The study of magnetic fields in the Sun is based on two fundamental works of the US scientist E. Parker (Parker, 1955, 1958), which actually determined all subsequent investigations of the solar activity. In those works, he proposed a model of the generation of the solar magnetic field (the so-called "Parker dynamo") and formulated the concept of the high-speed solar wind. It is interesting to note that both works were based on rather scanty experimental material. All the more surprising is the confirmation of Parker's main ideas and their enormous influence on subsequent research.

2 Solar wind, sector structure of the interplanetary magnetic field, and heliomagnetic equator

The amazing history of the publication of Parker's works according to recollections of his contemporaries is described in detail in (Obridko and Veisberg, 2017), including the criticism from the leading experts in this field, S. Chapman and G. Simpson, who denied the very idea of a dynamic atmosphere, the Parker's courageous opposition to their authoritative opinion, and the triumph when his calculations were confirmed.

The first evidence of the existence of the solar wind came from the Soviet research team headed by Prof. Gringauz, who reported observations of Lunik 2 launched in September 1959 (Gringauz et al., 1960, 1961) and the US missions Explorer 10 (Bridge et al., 1962) and Mariner 2 (Neugebauer and Snyder, 1962).

The next step was the simplest model of a tilted dipole (Schulz, 1973; Smith, Tsurutani, and Rosenberg, 1978), whose equator produces a sinusoidal heliospheric current sheet (HCS) symmetric about the heliographic equator.

Figure 1 represents the structure of the large-scale magnetic field. At the cycle minimum, the heliospheric current sheet lies in the plane of the solar equator, while at the maximum, it can be tilted up to 90°.

The discovery of the solar wind and the sector structure was not only of great practical importance, but also showed that processes in the near-earth space are closely related to processes in the Sun and, in fact, the study of the former allows some diagnostics of solar physics phenomena.

A typical structure of the heliospheric magnetic field is shown in Figure 2. Large dark regions are coronal holes. Above, directly on the line of the heliospheric equator, one can see a large active region.

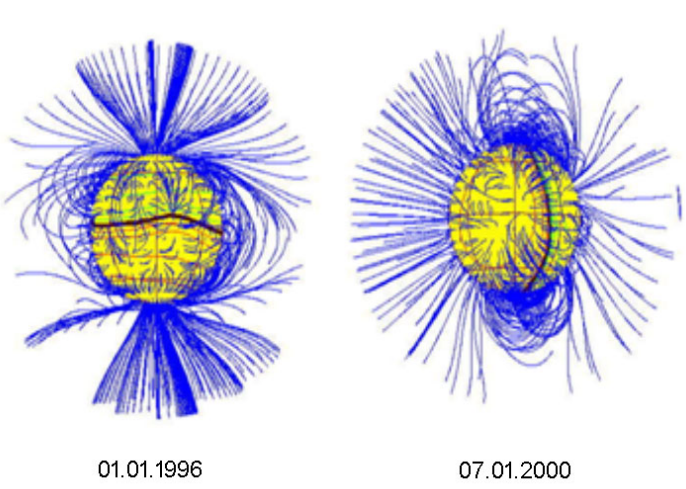


Figure 1 The force lines of a large-scale magnetic field in the vicinity of the minimum (01.01.1996, left) and the maximum (7.01.2000, right) of the 11-year cycle. The bold black line is the neutral line – the heliomagnetic equator.

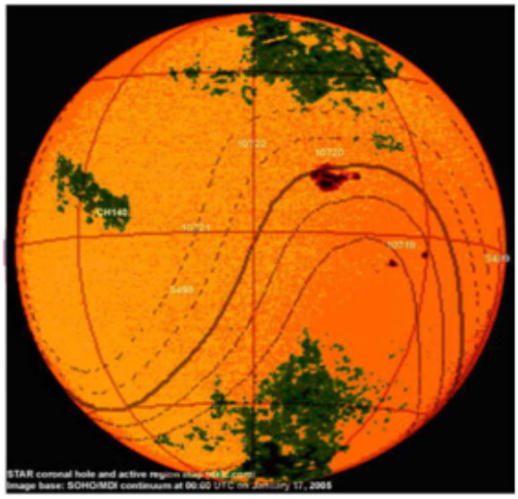


Figure 2 A typical structure of the heliospheric magnetic field.

The next important step was taken when the magnetograph data from the Mount Wilson Observatory covering the entire surface of the Sun were published. It became clear that the term "complexes of solar activity" was more adequate to characterize a long-term increase in solar activity in a certain range of longitudes lasting from several months to several years.

The distribution of magnetic fields outside sunspot groups was first considered in (Babcock and Babcock, 1955) for the period of the solar activity minimum 1952–1954. Besides establishing the existence of a polar magnetic field, the authors discovered two systems of magnetic fields at low latitudes: bipolar magnetic regions (BMOs),

coinciding with active regions and unipolar magnetic regions (UMOs), i.e., vast areas of the same field polarity.

This study was continued by W. Bumba and R. Howard (Bumba and Howard, 1965). They analyzed magnetic observations of the Mount Wilson Observatory for 4.5 years from August 1959 to the end of 1962 and from June 1963 to June 1964 and showed that a solar activity complex is evolving as follows. In a certain range of longitudes, no new activity is observed during several rotations, but diffuse fields of the old regions. Then, one or more new active regions (AR) appear and gradually expand in both latitude and longitude. It turned out that the largest group in a complex is usually the first to emerge. Moreover, large complexes have longer lifetimes and involve large groups.

For further investigations, it is important to note that the above-mentioned works, actually, formulated the notion of an active complex, which includes not only ARs, but also unipolar magnetic regions. This implies the need to include also the coronal holes and makes us speak of a global complex of activity.

At the time when magnetic fields all over the solar surface were measured at the American National Observatory under the leadership of Robert Howard, I worked for some time as a guest at the Ondřejov Observatory in Czechoslovakia and witnessed R. Howard and V. Bumba processing these data. They plotted giant diagrams, spread them on the floor, and painted them by hand, because then there were no good color printers. It quickly became clear that large-scale magnetic fields form stable structures on the surface of the Sun.

On the other hand, quite complete catalogs of active regions with proton flares were already available (Švestka, 1966, 1968). At that moment, V. Bumba and I came up with the idea to relate the most striking manifestations of solar activity, namely, proton flares with the sector structure. At first glance, it seemed that these phenomena were little related. Besides, the database was then insufficient. Nevertheless, we could find a spatial relation between both phenomena showing that active regions with proton flares are formed near the boundaries of the sector structure. This work (Bumba and Obridko, 1969) aroused great interest and was referred to in many publications.

It turned out that the higher the clustering of active regions near the sector boundaries, the more intensive the manifestations of activity are observed. Such clustering is a natural consequence of the general field structure in the Sun and in the heliosphere. In fact, the above-mentioned work was one of the first indications of a certain spatial priority of global fields in the general system of the solar magnetic fields.

3 Coronal holes

Coronal holes (CH) became the subject of active discussions in the early 1970s, when they were first observed in the UV and soft X-ray ranges on board the OSO-7 spacecraft and Skylab. In fact, Waldmeier (1950) had observed them earlier in the white light during eclipses, because due to their low density they emit less scattered light than high-density equatorial objects, and called them coronal "holes" (in German "locher"). Later on, they were identified with areas of reduced brightness in extreme ultraviolet and X-ray radiation. A detailed study of the size and location of these

areas revealed their relationship to the solar wind and geomagnetic activity (Harvey et al., 1975).

At present, coronal holes are regularly recorded by satellite and ground-based methods. On board the space missions, such as Yokho, SOHO, Koronas, SDO and Hinode, CH are observed in the X-ray and ultraviolet ranges. On the earth, they can be observed in the HeI 10830 line. It is important to note that in the X-ray and ultraviolet ranges, coronal holes are seen as regions of reduced radiation, and in the 10830 line, as an area brighter than the environment (Harvey et al., 1975; Zirin, 1975; Harvey and Sheeley, 1977; McCabe et al., 1977).

However, of particular interest are stable coronal holes at mid latitudes as elements of solar activity. Coronal holes usually occur in unipolar regions with a predominantly open magnetic field. It has been shown that the high-speed solar wind, which is responsible for geomagnetic disturbances, is associated with CH (Krieger et al., 1973; Sheeley et al., 1976; Kovalenko, 1983; Rozelot, 1983). A review of the physical conditions in CH is given in (Mogilevsky et al., 1997).

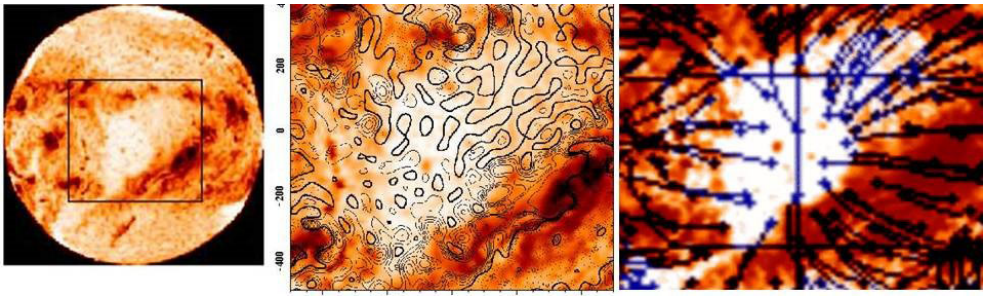


Figure 3 Structure of the coronal hole of 03.02.2002.

As shown by further studies, in addition to the open configuration of the global field, the emergence of a mid-latitude coronal hole requires the presence of an active region (AR) with strong local fields in the vicinity of the CH. The relationship between CH and AR was noticed when examining Skylab data (Levine, 1977). It was found (Wang et al., 1988) that the emergence of an open CH configuration is usually accompanied by the formation of two systems of closed field lines. Later, it was shown that changes in the CH boundaries and energy balance are sometimes largely determined by sporadic pulse-like fluxes of hot plasma ($T \geq 106$ K) and regular energy fluxes from the surrounding AR, as well as by the diffusion of X-ray "dots" through the CH boundaries (Shibata et al., 1994; Mogilevsky, 1995). The active region in the vicinity of the CH is dynamically and energetically related to the CH (Mogilevsky et al., 1997; Obridko, 1998). Figure 3 illustrates the structure of the coronal hole observed on the solar disk on 3 February 2002. On the left, there is a coronal hole on the disk; in the center – a larger-scale CH image, one can see the fine structure of brightness in the UV range and the magnetic field on the photosphere level; on the right, the calculated projection of divergent magnetic field lines.

3.1 The analogy between coronal holes and sunspots

The relationships described above point out a close analogy between sunspots (as observed in the photosphere) and coronal holes (see Figure 4). A sunspot is an object in local magnetic fields, and a coronal hole is a similar object in global magnetic fields. The similar features of coronal holes and sunspots are as follows:

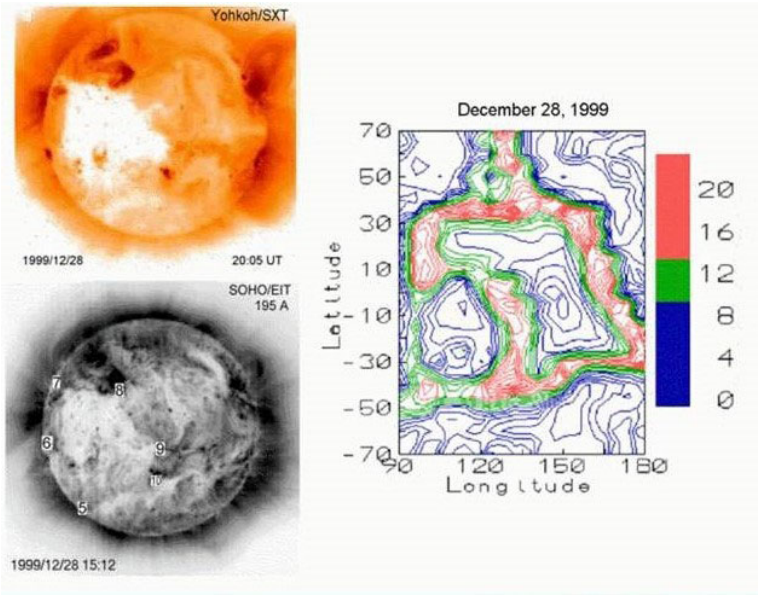


Figure 4 Coronal hole of 26.12.1999 in two spectral ranges. The magnetic field structure on the photosphere in the vicinity of CH is shown on the right.

(a) Location at the hills of the magnetic field.
(b) Deficiency of radiation in the optical range in sunspots and in the X-ray and UV ranges in CH simultaneously with its increase at the heights of radio emission.
(c) At the center of both objects there is an area with a vertical magnetic field, which is replaced at a certain height by a zone of intense expansion.
(d) Coronal holes have two zones similar to the sunspot umbra and penumbra. A rapid expansion at a certain height is determined by a sharp drop of external density. In coronal holes, the same effect arises as a result of the disappearance of the surrounding system of closed field lines.
(e) A system of converging field lines of the transverse magnetic field is observed in the immediate vicinity of sunspots and coronal holes (see the figures in (Mogilevsky et al., 1997; Obridko, 1998)).
(f) Intensive matter outflow. In the photosphere, it is an outward flow of matter in the penumbra, which changes its direction in the chromosphere. In CH, the matter outflow starts at relatively low altitudes.
(g) Sunspots usually form bipolar groups. Coronal holes can demonstrate a similar behavior. One can often observe CH shifted by $\sim 180^\circ$ in longitude. The magnetic fields in these CH are opposite in sign. Sometimes CH can be shifted by 90° maintaining their polarity.

Of course, there can be no complete analogy. The analogy is determined by the similar structure of the magnetic field. However, the characteristic sizes of these objects are not the same differing by 1–1.5 orders of magnitude. Besides, they are located in different layers of the solar atmosphere and, naturally, have different mechanisms of energy transfer and release.

3.2 Rotation of coronal holes

Soon after the discovery of coronal holes, scientists found out their seemingly paradoxical property – a solid-body type of rotation, i.e., a small latitude gradient of angular velocity. If we write down the differential rotation law in its classical form

$$V = A + Bsin^2\theta, \tag{1}$$

where V is the angular velocity (in this case, synodic), and θ is the latitude, it turns out that, for coronal holes, $B = \pm 0.4^\circ$/day. This sharply contradicts with the well-known Newton–Nunn result for sunspots, where $B = -2.6^\circ$/day.

The solid-body rotation of coronal holes had long been considered an established fact. It was mentioned in many monographs and textbooks and was widely used in practice. On the other hand, the following circumstance was not taken into account. It is true that the rotation of CH differs from that of sunspots; however, it should be compared not with sunspots, but with the corona, which rotates more rigidly, and the rotation of which depends both on the level of activity and on the phase of the cycle.

The conclusion about the "solid-body" rotation of coronal holes was based on Skylab observations for a short period in 1973, i.e., two to three years before the sunspot minimum. The analysis of CH rotation for 1978–1985 shows that it is an incorrect generalization of a particular case. The fact is that coronal holes near the maximum and at the beginning of the declining phase show quite a noticeable differential rotation. Then, the differentiality decreases gradually, and the process starts from high latitudes, i.e., the high-latitude parts of coronal holes begin to rotate faster.

Coronal holes are not unique to the solar corona. The entire corona rotates in exactly the same way and with approximately the same quantitative characteristics. The rotation becomes most rigid at the decline of activity about three years before the minimum. It is steadily fixed in approximately the same phase in all cycles. The period of the greatest gradient of differential rotation is also established with confidence. This is the growth phase approximately 1–1.5 years before the activity maximum. Thus, we can suggest that the differential rotation of coronal holes and the solar corona as a whole largely reflects the rotation of the coronal inner layers (Obridko and Shelting, 1987 a, b; 1988 a, b; 1989; 1990).

3.3 Global complexes of activity

The study of global complexes of solar activity requires the use of large sets of data, including the characteristics of both local and global fields, information on photospheric, chromospheric, and coronal processes, and even heliospheric and geomagnetic

disturbances, collected during long time intervals. This is partly why the notion of a complex of activity has fallen out of use. Nowadays, the researchers prefer to deal with "complexes of active regions" or even "complexes of sunspot groups", the study of which does not require large amounts of data and, most importantly, which are not supposed to have long lifetimes. So, the "complex of active regions" was defined as a set of two or more active regions that are connected by a common magnetic field and whose evolution reveals a relation and interaction between their components or individual parts (Ishkov and Mogilevsky, 1983; Obridko, 1985; Mogilevsky and Shilova, 1998). A somewhat different but close definition is given in the extensive monograph (Yazev, 2014).

3.3.1 General description of a global complex of activity

In the course of evolution, the large-scale open magnetic field (OMF), coronal holes, and active regions form a single complex with the following properties (see Figure 5).

1) In the regions, where the magnetic field in the chromosphere and the lower corona deviates from the radial direction by $<20°$, there appear optical and X-ray coronal holes. Despite the physical identity of all these objects, their boundaries may not fully coincide and the appearance of coronal holes may be delayed relative to the appearance of OMF.
2) In two or three rotations after the appearance of coronal holes, their shape and size begin to change under the influence of active regions located between the conjugate coronal holes. As a result, a "saddle"-type configuration appears in the transverse field at the level of the photosphere in the vicinity of the CH boundaries. Outside the photometric coronal hole, the magnetic field vectors converge to the conjugate active regions to form a single complex of activity. This effect is especially well pronounced in powerful active regions.
3) The lifetime of coronal holes ranging from 2–3 rotations to 1.5 years exceeds the lifetime of the associated active regions. As the active regions weaken or disappear, the coronal holes change accordingly.

Certain difficulties arise when comparing the positions of coronal holes and active regions on the disk. The point is that it is not clear *a priori* what should be considered the boundary of a coronal hole even when observed at the same wavelength. In a number of works, this problem was studied in detail for coronal holes observed at the wavelength of 284 nm. The situation becomes even more complicated when comparing observations at different wavelengths.

A coronal hole arises in the OMF zone, where the field lines of the large-scale field are mainly radial. With the distance from the zone of strictly radial large-scale field, the tilt of the field lines in the surrounding photosphere increases. The coronal hole exists until the tilt reaches 20°, although its contrast is gradually weakening. A feature appears that can be called the CH penumbra. Then, starting with the tilt of 50°, the brightness of the environment returns to the level of the undisturbed chromosphere. The region with the tilt of the field lines between 20° and 50° is just where the active regions conjugated with the coronal hole are located.

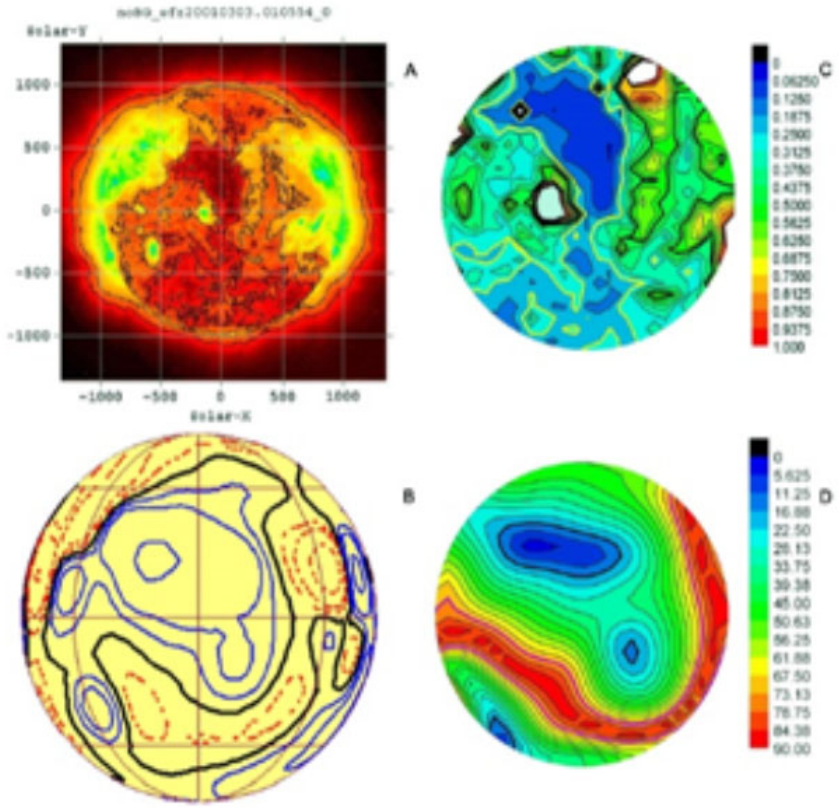


Figure 5 The photometric and magnetic structure of CH of March 3, 2001. Panel A shows the original image. Panel B shows the structure of the radial magnetic field at 1.1 $R_\odot$ from the center of the Sun (calculations based on SWO data). Blue lines correspond to the positive polarity and dashed red lines, to the negative polarity. Panels C and D show only the central part of the solar disk at $R_\odot$. On panel C, the thick yellow and black lines delimit the areas where the brightness is below 0.25 and 0.50 of the mean brightness on that day, respectively. Panel D shows the deviations of the field lines from the radial direction at 1.1 $R_\odot$ in degrees; the thick black and yellow lines show deviations of $<20^\circ$ and $<75^\circ$, respectively.

Another condition for the occurrence of coronal holes at mid-latitudes, besides the open configuration of the global magnetic field, is the presence of active regions with a strong local field in their vicinity. The relationship between coronal holes and active regions was established in early works based on Skylab data. The emergence of the open field of coronal holes is usually accompanied by the formation of two closed systems of field lines. Later on, it was shown (Shibata, 1994; Mogilevsky, 1995) that changes in the CH boundaries and energy balance may be largely determined by sporadic and pulse-like fluxes of hot plasma ("X-ray jets"), as well as by regular energy fluxes from the surrounding active regions. Active regions in the vicinity of coronal holes can be connected with the latter either dynamically or energetically. The magnetic field is generated at the base of the convection zone as a result of

interaction of the poloidal magnetic field and differential rotation (Ω-dynamo). This field emerges from the tachocline in the equatorial zone, perhaps, in the form of individual flux tubes, and manifests itself as active regions. At the same time, a wave that can be identified with the Maunder butterflies runs from mid-latitudes to the equator.

4 Quantitative analysis of the structure of large-scale fields over long time intervals

The main difficulty in analyzing cyclic variations of the global magnetic fields and heliosphere is connected with the limited data series. We have used photospheric magnetic maps for August 1959 – December 1978 (CR 1417–1648) obtained under the guidance of R. Howard at the Mt. Wilson Observatory (MWO). Another series of observation data was obtained at the Kitt Peak Observatory (KPO) under the guidance of J. Harvey during the period from January 1975 through July 1984 (CR 1622–1751). The third series of data was obtained at the John Wilcox Stanford Observatory (WSO) and was made available to us by courtesy of T. Hoeksema. The collection of these data started in May 1976 (CR 1641) and has continued till the present. When magnetic field measurements in the photosphere are available, the source surface field (i.e., the field at the base of the heliosphere) can be calculated under potential approximation in terms of the source–surface hypothesis. In spite of their obvious inhomogeneity, we have used all three data series. The data were reduced to the same scale by comparing the overlapping time intervals. We have used the McIntosh Hα magnetic maps for 1964–1974 (McIntosh, 1979) to reconstruct the source–surface magnetic field. The maps for later periods were adopted from Solar Geophysical Data. For cycles 15–20 we took the data published by Makarov and Sivaraman (1989 a, b). On the synoptic maps, the sign reversal latitudes determined by the McIntosh method from the location of large-scale filaments were marked at 10° intervals on each longitude. The signs on each synoptic map were marked proceeding from the magnetic field polarity on the north pole. Here, the sign remains constant between two field reversals in the neighboring solar cycles. Thus, we obtained synoptic maps similar to those published by Hoeksema and Scherrer (1986) and Hoeksema (1991). A standard method can be applied afterwards to calculate the source–surface magnetic field.

4.1 The basic equations and formulation of the problem

All components of the magnetic field at any point of a spherical layer from the photosphere to the so-called source surface can be calculated under potential approximation from observations of the longitudinal field. The source surface is by definition a spherical surface, where all field lines are radial. It is supposedly located at a distance of $R_s \simeq 2.5R_\odot$ from the center of the Sun. The equations for calculating the magnetic field components are written as follows:

$$B_r = \sum P_l^m(cos\theta)(g_{lm}\cos m\varphi + h_{lm}\sin m\varphi) \times ... \\ ... \times \left((l+1)(R_\odot/R)^{l+1} - l(R/R_s)^{l+1}c_l\right), \quad (2)$$

$$B_\theta = -\sum \frac{\partial P_l^m(\cos\theta)}{\partial\theta}(g_{lm}\cos m\varphi + h_{lm}\sin m\varphi) \times ... \\ ... \times \left((R_\odot/R)^{l+2} + (R/R_s)^{l-1}c_l\right), \quad (3)$$

$$B_\varphi = -\sum \frac{m}{\sin\theta} P_l^m(\cos\theta)(h_{lm}\cos m\varphi - g_{lm}\sin m\varphi) \times ... \\ ... \times \left((R_\odot/R)^{l+2} + (R/R_s)^{l-1}c_l\right). \quad (4)$$

Here, $0 \le m \le l < N$ (usually, $N = 9$), $c_l = -R_\odot/R_s)^{l+2}$, P_l^m are the Legendre polynomials, and g_{lm}, h_{lm} are the harmonic coefficients. The latter were partly received from T. Hoeksema and partly were calculated by ourselves from the WSO Stanford data. To find the harmonic coefficients g_{lm} and h_{lm}, and thus, to fully determine the solution, we had to use the following boundary conditions. As the lower boundary condition we usually adopted the synoptic map constructed from observations of the longitudinal field component in the photosphere ($r = R_{phot}$). The upper boundary is the source surface, where all field lines are radial.

These calculations are based on a few non-obvious assumptions. The most important is that the magnetic field from the photosphere up to a surface called usually the source surface is energetically stronger than any motion, there are no currents in the medium, and, therefore, the potential approximation can be used. In fact, this assumption is not quite true and is applicable only to medium and large scales.

The next assumption follows from the mathematical constraint, according to which, to solve the problem, it is necessary to know the normal component at the boundaries of the layer. In the photosphere, we have only line-of-sight measurements of the magnetic field. At the source surface (which, generally speaking, may be neither thin nor spherical), we assume, proceeding from the solar wind concept, that the field lines are stretched out by the solar wind, become radial and, accordingly, the potential is zero. The radius of the source surface was selected experimentally to fit the measurements of the interplanetary magnetic field and is most often taken equal to 2.5 radii of the visible surface of the Sun.

As concerns the photosphere surface, we can assume it to be current-free (which, strictly speaking, is wrong), obtain formulas for the line-of-sign field from equations (1–3), and find the undefined coefficients using the orthogonality of the Legendre functions or the least squares method. We can also assume that the field on the photosphere is initially radial (which is incorrect, too). Then, the photosphere surface is excluded from the region of potentiality, but the normal component can be found from the line-of-sight component by a simple rheometric transformation.

The task becomes even more complicated, when we want to use data from different magnetographs within the frames of a single database or, even more so, if we include magnetic data reconstructed from Hα observations.

During the past 50 years, these problems were discussed in a large number of publications (Altschuler and Newkirk, 1969; Schatten et al., 1969; Hoeksema and Scherrer, 1986; Wang and Sheeley, 1992, 2000; Obridko et al., 1996, 2004; Svalgaard et al., 1978; Wang and Sheeley,1992, 2000; Wang et al., 1998; Ulrich, 1992; Snodgrass et al., 2000; Demidov, 1998, 2002). Here, we are not in a position to discuss these works in detail. A thorough analysis of most of them is available in Obridko and Shelting (1999), Obridko et al. (2004, 2006).

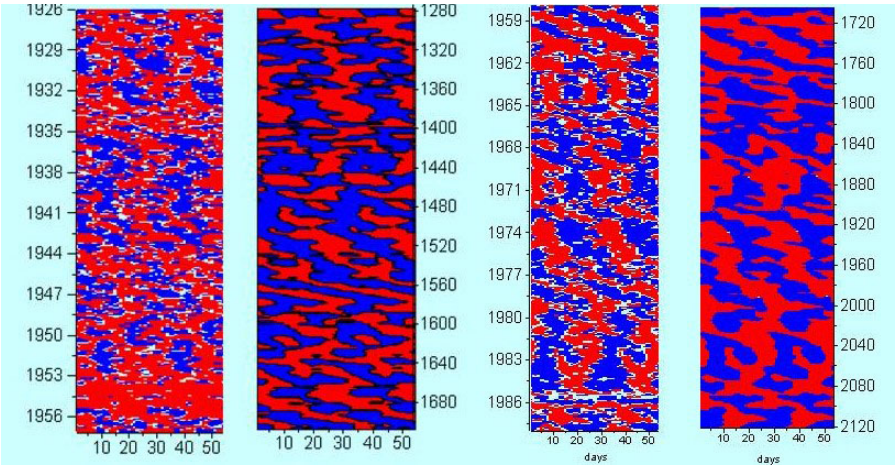


Figure 6 Polarity of the interplanetary magnetic field as inferred from ground-based and satellite data (first and third columns) and from data on the solar magnetic field.

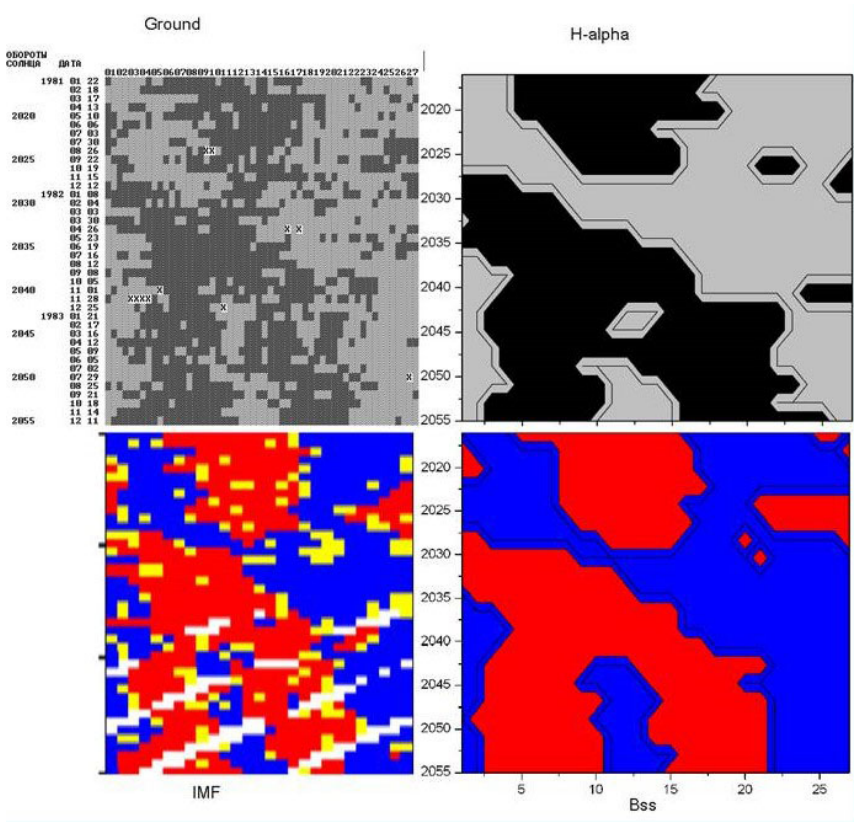


Figure 7 The polarity of the interplanetary magnetic field as inferred from ground-based (left-hand panel, top) and spacecraft (left-hand panel, bottom) data. The right-hand panels represent the results of strong smoothing of Hα observations and direct magnetographic measurements.

On the whole, it can be considered that, despite all the assumptions, the adopted method quite adequately describes the structure of the large-scale magnetic field and its manifestations in the corona and interplanetary space. The quantitative estimates of the field values are somewhat worse. Calculations within active regions performed by this method give only a rough approximation.

Figure 6 compares the polarity of the interplanetary magnetic field as inferred from ground-based and satellite data and from data on the solar magnetic field.

Figure 7 represents the polarity of the interplanetary magnetic field as inferred from direct measurements and from calculations.

4.2 Indices of the global magnetic field

A quantitative index that can be introduced for global fields is the energy index. To analyze cyclic variations of the global solar magnetic field, it is convenient to introduce magnetic indices, which are the quantities determined by the global distribution.

Let iB_r denote the squared radial component of the magnetic field averaged over the solar surface $\langle B_r^2 \rangle$:

$$i(B_r)|_R = \langle B_r^2 \rangle, \tag{5}$$

where R is the radius of the sphere, over which the averaging is performed. For the photosphere surface ($R = R_\odot$) and the source surface ($R = R_s$), we have, respectively:

$$B_r|_{R_\odot} = \sum_{lm} P_l^m(\cos\theta)(g_{lm}\cos m\varphi + h_{lm}\sin m\varphi)(l + 1 + l\zeta^{2l+1}), \tag{6}$$

$$B_r|_{R_s} = \sum_{lm} P_l^m(\cos\theta)(g_{lm}\cos m\varphi + h_{lm}\sin m\varphi)(2l + 1)\zeta^{l+2}, \tag{7}$$

where l and m are the indices of the spherical harmonics, $R_\odot$ is the radius of the Sun, $R_s = 2.5R_\odot$ is the radius of the source surface, $\zeta = R_\odot/R_s$, and P_m^l is the Legendre polynomial; g_{lm} and h_{lm} are tabulated in (Hoeksema and Scherrer, 1986).

Applying the averaging procedure (5) to equations (6) and (7) yields the following expressions for the indices $i(B_r)|_{R_\odot}$ and $i(B_r)|_{R_s}$ (Obridko and Yermakov, 1989):

$$i(B_r)|_{R_\odot} = \sum_{lm} \frac{(l + 1 + l\zeta^{2l+1})^2}{2l + 1}(g_{lm}^2 + h_{lm}^2), \tag{8}$$

$$i(B_r)|_{R_s} = \sum_{lm} (2l + 1)\zeta^{2l+4}(g_{lm}^2 + h_{lm}^2). \tag{9}$$

Let us also introduce partial field indices, namely, zonal even, ZE ($m = 0$, $l = 2k$); zonal odd, ZO ($m = 0$, $l = 2k + 1$); sectorial even, SE ($m = l = 2k$); and sectorial odd, SO ($m = l = 2k + 1$). These indices are determined from equations (8) or (9) taking into account the limitations on m and l mentioned above.

A strong dependence of indices on the height R can be used as a spatial filter. The source surface calculations give us the largest scale fields. Imposing limitations on l or m, we can isolate the contribution of fields of different types of symmetry: zonal, sectorial, axisymmetric, even and odd with respect to the equator or to the rotation axis.

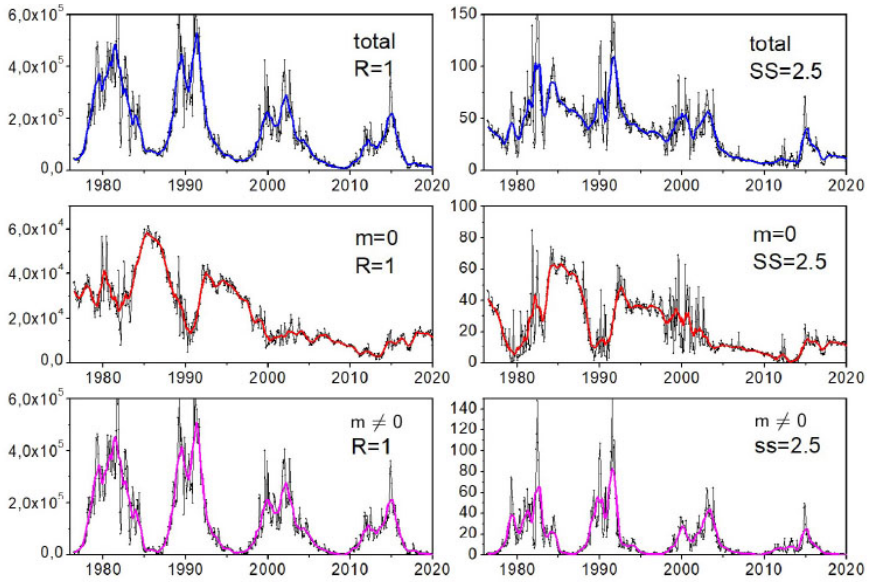


Figure 8 $i(B_r)$ index for the photosphere (left panel) and for the source surface (right panel). All values are in microtesla squared. The black curves are drawn in every half of the Carrington rotation; the color curves represent smoothing over 13 points.

Figure 8 shows the $i(B_r)$ index for the photosphere and for the source surface. If we compare the two plots, we will also see here an 11-year periodicity. The phases of the maxima mainly coincide, though the Gnevyshev dip at the cycle maximum is seen more clearly in the large-scale field. As a result, the secondary maximum is more clearly pronounced, too. The maxima of the global magnetic field are shifted by 2–3 years relative to the sunspot maxima.

One can also see other features such as a gradually decreasing activity of the fields of all scales. This decrease makes us believe that we are on the eve of a very low cycle. At first glance, the decrease is approximately the same in the photosphere and at the source surface. However, this is not exactly so.

The axisymmetric component, $m = 0$, behaves in a completely different way. First of all, the decrease in the height of every subsequent cycle compared to the previous one is much more pronounced. The maxima themselves are shifted relative to the maxima of the local fields. Moreover, cycle 23 (1997–2008) is hardly noticeable at all.

To assess the contribution of different components, we can use the index of the effective multipole introduced in our earlier work:

$$I_M = -0.5 \log(i(B_r)|_{R_s}/i(B_r)|_{R_\odot})/\log(2.5). \quad (10)$$

It is determined as the logarithm of the ratio of $i(B_r)$ at the source surface to its value in the photosphere (Ivanov et al., 1997). In fact, when passing from the photosphere to the source surface, the mean square radial component of the magnetic field changes in accordance with the power function $\sim R^{2n}$, i.e., $\sim(1/2.5)^{2n}$, where $n = 3$ for a dipole source, $n = 4$ for a quadrupole source, and $n > 4$ for a higher-order

multipole source. When the field under discussion is a combination of fields from several sources with different weight, n can assume values from 3 to 4 (in the case of combined dipole and quadrupole sources) or higher (in the case of a higher-order multipole field).

4.3 Correlation between the fields of different scales and their relationship with other heliogeophysical indices

In the previous Section, the indices were calculated by averaging the squared field over a sphere of radius R. Alternatively, we can average the field over a solar hemisphere on a given day and then find the mean square fields over one rotation. In fact, this is equivalent to using as directly observed field the value of the magnetic field of the Sun as a star, which is measured at Stanford and regularly published in Solar Geophysical Data. This new index will be henceforth called the index of the mean magnetic field (Shelting et al., 1989). It is defined as the squared magnetic field of the Sun as a star averaged over one rotation:

$$i(\overline{B}_{\|}) = \langle \overline{B}_{\|}^2 \rangle = \frac{\sum_{k=1}^{27} (\overline{B}_{\|})_k^2}{27}. \tag{11}$$

Figure 9 illustrates the cyclic curve of this index along with the index of the source surface field $i(B_r)|_{R_s}$. Both curves are very much alike. It should be emphasized that $i(B_r)|_{R_s}$ is derived from the radial component of the source surface field ($R = 2.5R_{\odot}$) under the potential field assumption, while $i(\overline{B}_{\|})$ is calculated using the observed longitudinal component of the Sun as a star. Mathematical averaging in the former case is not equivalent to the instrumental averaging during the observation of the Sun as a star in the latter, and, therefore, the averaging ranges are different. So, it would be not surprising if the curves had nothing in common. The more interesting is their close similarity. Note that the values of $i(\overline{B}_{\|})$ in Figure 9 are reduced by a factor of 50.

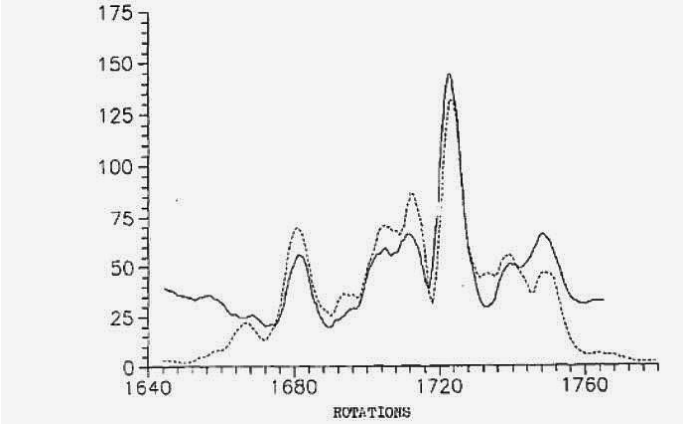


Figure 9 Cyclic variation of $i(\overline{B}_{\|})$ plotted from the Stanford routine data on the mean longitudinal magnetic field of the Sun as a star (dashed line) and $i(B_r)|_{R_s}$ (solid line).

Table 1 Correlation coefficients.

Indices	R_z	CaII plage 1	CaII flux F	X-ray	aa-ind.	Corona CI	$i(B_r)\|_{R_\odot}$	$i(\overline{B}_\parallel)$	$i(B_r)\|_{R_s}$
Sunspot number, R_z	1.00	0.98	0.83	0.94	0.15	0.74	0.95	0.74	0.15
Photospheric magnetic index, $i(B_r)\|_{R_{\odot\|}}$	0.95	0.90	0.84	0.96	0.01	0.81	1.00	0.77	0.33
Mean solar magnetic index, $i(\overline{B}_\parallel)$	0.74	0.68	0.60	0.88	0.65	0.97	0.77	1.00	0.81
Source surface magnetic index, $i(B_r)\|_{R_s}$	0.15	0.15	0.43	0.42	0.73	0.70	0.33	0.81	1.00

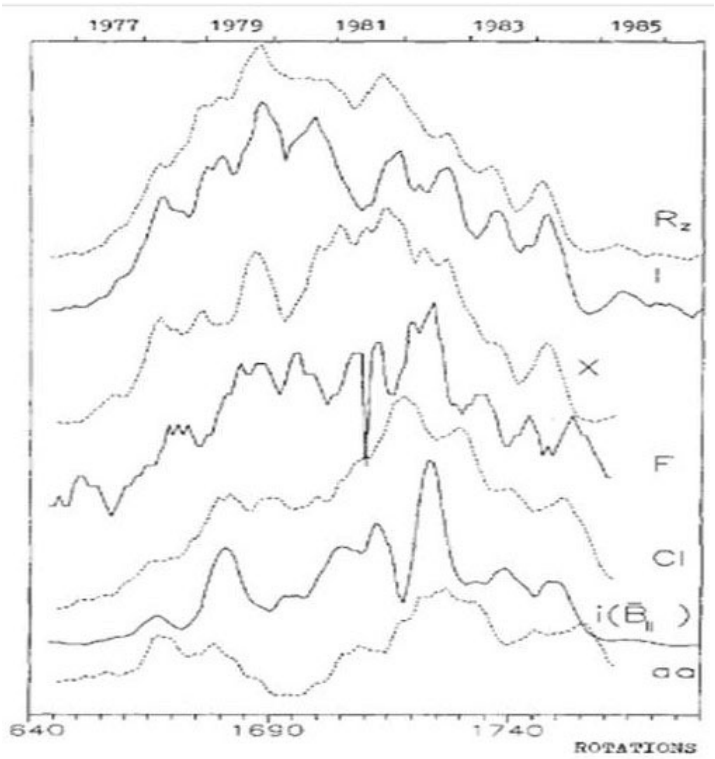


Figure 10 Cyclic variation of some heliogeophysical indices: the Wolf number, R_z; the CaII K plage index, I; the 1–8 Å solar X-ray flux, X; the CaII K full-disk flux, F; the coronal index, CI; the mean solar magnetic field index, $i(B_\parallel)$; and the geomagnetic aa-index.

As seen from the plots above, from Table 1 and Figure 10, photospheric magnetic fields have a good correlation with the mean indices of local phenomena in the Sun, such as active regions, sunspot groups, and monthly mean X-ray fluxes. The global fields correlate more closely with geomagnetic disturbances as follows from their relationship with the mean characteristics of the solar wind.

The solar corona index stands apart. The fact is that two alternative mechanisms are competing in the corona heating theory. One is determined by the dissipation of magnetic fields and is associated with local structures. The other is a wave mechanism more closely related to large-scale fields. Both mechanisms actually work, but their relative contribution varies depending on the phase of the cycle and latitude on the Sun (Badalyan and Obridko, 2006, 2007).

4.4 Cyclic variations of different magnetic field components

Figure 11 represents a map of the azimuthal component for cycle 23. To test the validity of the Hale law for large-scale fields, we estimated the area occupied by the field lines directed westwards or eastwards. It turned out that the anti-Hale area (yellow region) was larger than the Hale area (blue region) and the Hale intensity was higher than the anti-Hale intensity. Thus, the generalized Hale law can be formulated as follows: in the odd cycles in the northern hemisphere, the area occupied by the field lines directed westwards is, on the average, smaller than the area occupied by the eastward field lines. However, the strength of the field with westward lines (N-polarity of the leader spot in odd cycles in the northern hemisphere) is larger than the strength of the field with eastward lines. This rule is equally valid for the local and global fields.

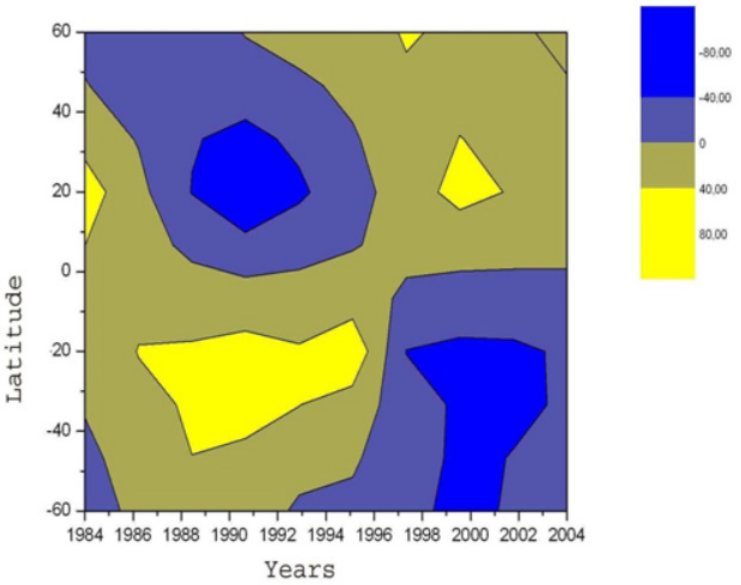


Figure 11 A map of the azimuthal component for cycle 23.

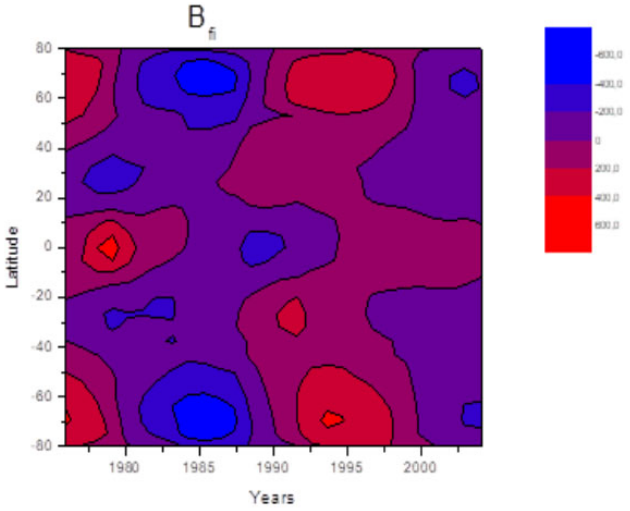


Figure 12 The map of the magnetic-field meridional component.

The map in Figure 12 demonstrates the existence of dipoles and quadrupoles. One can see that the whole structure is quite complicated and, in certain time intervals, three zones are present in each hemisphere instead of just the zones of opposite polarity.

Figure 13 represents magnetic data (the light elements correspond to the north polarity; the dark ones – to the south polarity). One can see a wave of local fields (Maunder butterflies) moving from mid latitudes to the equator and a poleward meridional wave, which results in the reversal of the polar field. This reversal occurs in the vicinity of the maximum of the cycle of local fields. The new field forms the basis of a new cycle. However, the cycle of local fields and that of the polar field do not evolve in anti-phase; i.e., the cycles at different latitudes are imposed on each other. A non-standard situation arises when three stripes are seen in each hemisphere. As a

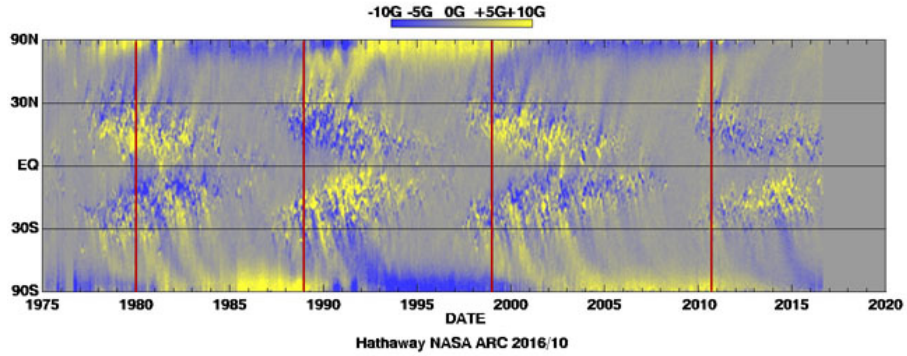


Figure 13 Magnetic data (the light elements correspond to the north polarity; the dark ones – to the south polarity).

result, the zonal harmonic $L = 5$ intensifies. The dates of these specific maxima are marked in the figure with thick red lines. These maxima correspond to a short-term situation when two waves of a new cycle appear on the Sun in each hemisphere, but the wave of the previous cycle still exists in the polar zone. It is seen that the time from our marks to the complete polarity reversal of the polar field is 1–2 years.

4.5 Polarity reversal of the polar magnetic field, its meaning

The reversal of the polar magnetic field occurs due to the transport of the magnetic flux as a result of turbulent diffusion, meridional circulation, and differential rotation and energy release in the solar corona. The evolution of the weak (or background) magnetic field leads to the sign reversal of the polar field, which is shifted in time relative to the reversal of the strong local fields. As a matter of fact, the field reversal is a phenomenon, which has a physical meaning only in the case of the dipole magnetic field. We can isolate the dipole magnetic field from the overall variation and examine its change during an activity cycle (Fig. 14).

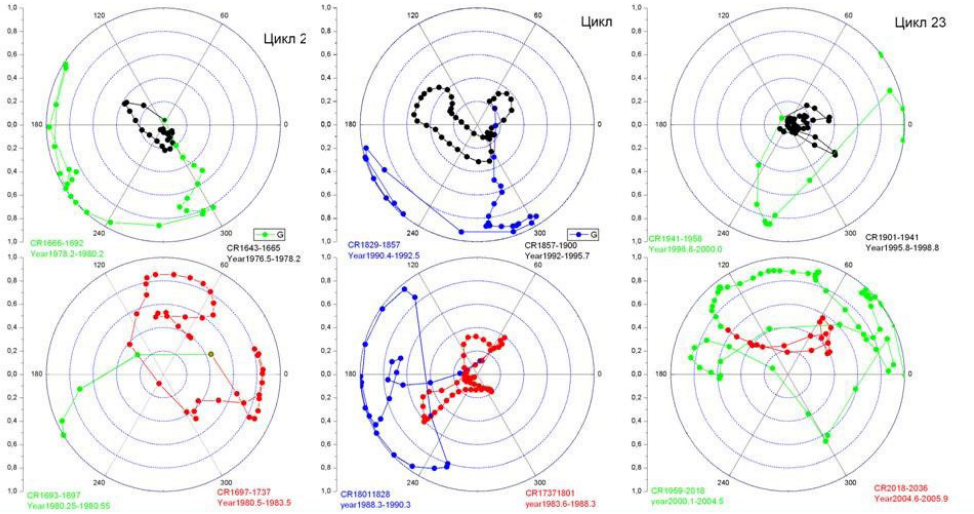


Figure 14 Position of the north pole of the magnetic dipole for three solar cycles. The upper panels correspond to the northern hemisphere and the lower ones, to the southern hemisphere. The circles are the contour lines for the values of $\cos\theta$ given on the scales for each cycle.

One can see that, during the cycle minimum, the pole of the dipole makes rather regular, precession-like motions completing one or two revolutions around the solar rotation pole. The quasi-precession accounts for the fact that variations with a period of 1.5–2.5 years are not only observed in the epochs of high activity, but also remain noticeable on the quiet Sun.

This quasi-precession lasts from one to three years. Then, we see a sudden jump during 0.7–1.2 years to the equatorial region, where the dipole continues a smooth

motion along the longitude for another 1.5–3 years. This is followed by a new jump, and the precession goes on around the opposite pole.

It is important to note that only the axisymmetric part of the dipole vanishes at the moment of the polarity reversal ($l = 1$, $m = 0$, see formulas 2–4). The dipole with the axis in the equatorial plane (a "horizontal" dipole with nonzero coefficients g_{11} and h_{11}) continues to exist, although it decreases somewhat in magnitude (Livshits and Obridko, 2006).

4.6 Mutual relationship between the dipole and quadrupole

The second most important harmonic in the expansion of a large-scale field is the quadrupole. Figure 15 shows the ratio of the magnetic moments of the quadrupole and the dipole. One can see that the relative contribution of the quadrupole fell steadily over cycles 21–23; however, in the nighttime in cycle 24, it was becoming comparable in size to the dipole. This indicates an unusual character of the current period. Perhaps, we are witnessing the beginning of a period of relatively low solar activity.

Note that, unlike the dipole, the quadrupole is even relative to the solar heliographic equator. This leads to the north–south asymmetry of activity in the Sun and a shift of the heliomagnetic equator (see Figures 1–2 in Section 2). It can be detected both directly from averaged solar observations and from the position of the heliospheric current sheet.

Mursula and Hiltula (2003) analyzed direct observations of the IMF polarity for 1965–2001 and found out that, in the epochs of the solar minimum, the polarity corresponding to the northern hemisphere is observed more frequently than the polarity typical of the southern hemisphere. A conclusion was drawn that the HCS moves south at the solar minimum. This effect was called a "Bashful Ballerina", since it looks as if "the solar ballerina is pushing her excessively high flaring skirt downward" whenever the solar activity is fading away.

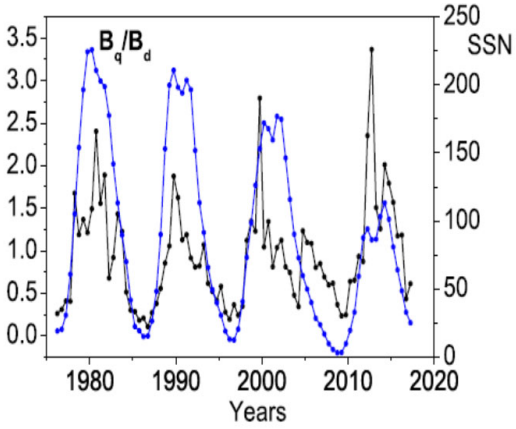


Figure 15 The ratio of the mean semiannual values of the magnetic field of the solar quadrupole B_q to the mean semiannual values of the magnetic pole of the solar dipole B_d. The blue curve shows sunspot numbers (Obridko et al., 2020).

Thus, the heliospheric current sheet undergoes variations of two types. Mathematically, the position of HCS is determined by calculating the uppermost latitude of the neutral line of the large-scale magnetic field at the source surface. Then, the southern (negative) latitude T_S is subtracted from the northern latitude T_N and the mean value is taken. In fact, this is how the heliospheric equator is found. This procedure involves only the odd, anti-symmetric harmonics of the global field multipoles.

The even (quadrupole and higher-order) harmonics that do not change the sign when passing over the equator lead to the asymmetry of HCS. Thus, we have a shift, ΔT, of HCS with respect to the solar equator. Mathematically, this shift is determined as half the sum of T_N and T_S. Note that the southward shift described by Mursula and Hiltula (2003) gives T_S larger in absolute value than T_N and, therefore, $\Delta T < 0$.

We calculated the annual mean T_N and T_S and, then, ΔT for 1915–2000. The center of gravity of the heliospheric current sheet oscillates with a quasi-period close to 11 years.

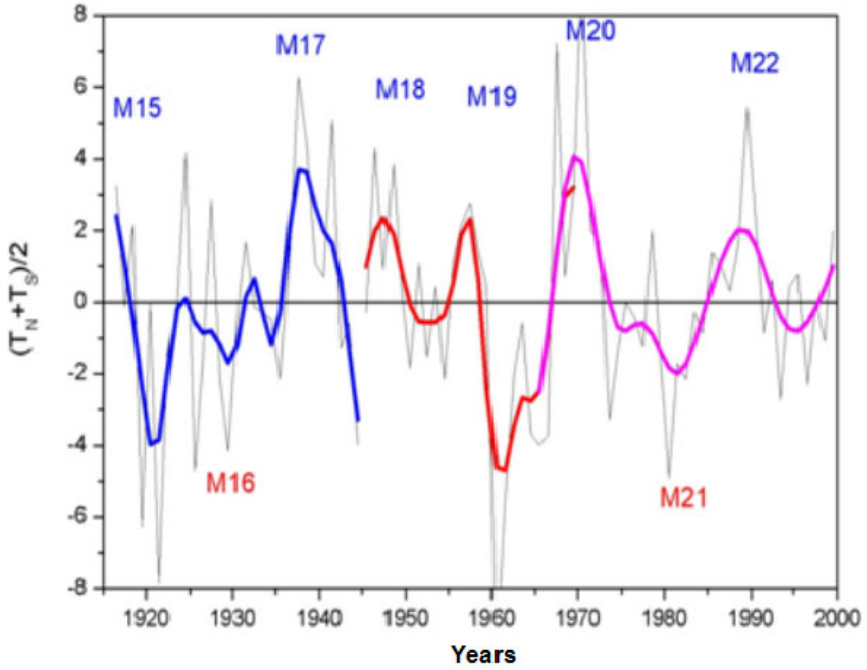


Figure 16 Position of the heliospheric current sheet relative to the equator in the time interval of 1915–2000.

The curve minima lie usually in the negative half-plane and are often close to the minima of the solar cycles. This corroborates the results obtained by Mursula and Hiltula (2003). Besides that, an additional effect is observed: the values of ΔT near the cycle maxima are mostly positive, indicating that the HCS is shifted north. Sometimes, the curve in the vicinity of the maximum does not pass over zero, but ΔT at the maximum is always larger than it is at the minimum (Obridko and Shelting, 2008) (see Figure 16).

4.7 Rotation of the magnetic field and its relationship with differential rotation

It should be noted that, as seen from Figure 16, the dipole poles shift in latitude during the cycle. The same happens to the poles of a quadrupole. Since the Carrington reference frame is calculated for a single latitude and does not take into account the differential rotation, the poles rotate faster than they would do in the case of solid rotation. Hence, a picture arises showing an accelerating or decelerating movement of the poles. Simultaneously, the latter can also shift relative to each other (see Figure 17).

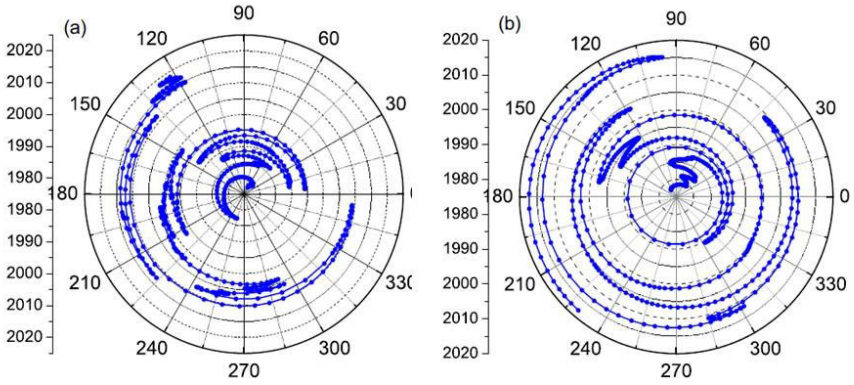


Figure 17 Longitude–time diagram for the dipole (a) and quadrupole (b) (Obridko et al., 2020).

In this context, it seems reasonable to compare long-term variations in the rotation of the system of large-scale fields with the solar activity determined by the sunspot number. For this purpose, the entire data series is used, including the reconstructed data (see Figure 18).

The rotation of the source–surface global field decelerates as the activity of the local fields grows during both the 11-year and longer cycles. The rotation periods

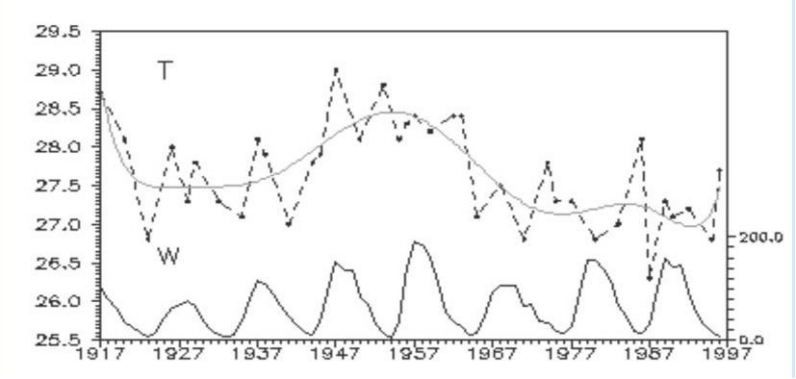


Figure 18 The rotation period as a function of the 11-year cycle.

were maximum at the middle of the 20th century, i.e., in the period of the high cycles 18 and 19.

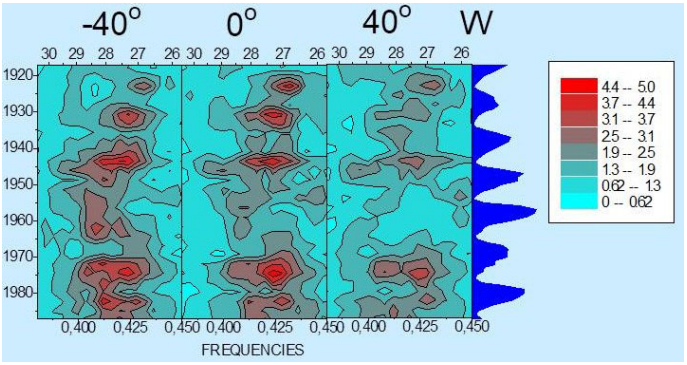


Figure 19 Relationship between the angular rotation rate and solar activity at different latitudes.

Note that this effect is also noticeable on a smaller time scale. At the minimum of the cycle, the frequency increases, i.e., the rotation rate increases. Moreover, this effect is pronounced both at low and at mid latitudes. Hence, it cannot be a simple effect of the latitudinal shift of the poles (see Figures 19–20).

Thus, we are dealing with a somewhat unexpected effect of negative correlation between the solar activity and the rotation rate of the Sun (Obridko and Shelting 2000 a, b; 2001). Having analyzed the daily Doppler measurements over the period from 1967 to 1976, Howard (1976) concluded that the angular rotation velocity of the Sun at the equator reached its maximum precisely at the minimum of the cycle

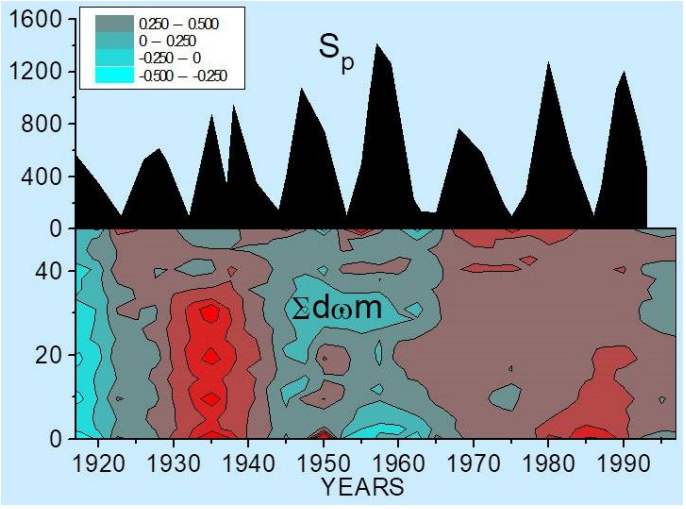


Figure 20 Deviations of the angular rotation rate from the differential rotation rate depending on the solar activity level.

in 1976. Based on data from the National Astronomical Observatory of Japan for 1954–1986, Kambry and Nishikawa (1990) showed that the equatorial rotation rate was decreasing gradually from the beginning of the cycle (i.e., from the epoch of the minimum) to its end. This effect was confirmed later on the basis of up-to-date data in (Obridko and Shelting, 2016).

Conclusions

So, in the past 50–70 years, a change occurred in the concept of the large-scale magnetic field in the Sun. If earlier the large-scale field was considered a secondary product of the evolution of active regions arising as a result of the decay of spots and disappearance of plumes, now we understand that it is a primary process of generation of solar magnetic fields. The up-to-date concept of the mean-field dynamo suggests that the magnetic field is generated by differential rotation at the base of the convection zone. It is still not clear how this field is converted to individual objects such as sunspots. One of the theories was proposed by Israeli astronomers, who consider the occurrence of the observed phenomena of solar activity, such as sunspots, within the general scheme of the dynamo process.

This dynamo model takes into account the algebraic and dynamic nonlinearities of the α-effect, where the equation for the dynamic nonlinearity is derived from the conservation law for the magnetic helicity. The budget equation for the evolution of the Wolf number (Kleeorin et al., 2016) is based on a sunspot formation mechanism related to the negative effective magnetic pressure instability (Kleeorin et al., 1989). This instability redistributes the magnetic flux produced by the mean-field dynamo (Rogachevskii and Kleeorin, 2007; Brandenburg et al., 2016). This dynamo model demonstrates very rich behavior, reproducing the observed evolution of the magnetic activity during the past three centuries.

The reverse branch of generation of the poloidal field from the toroidal one (the so-called α-dynamo) has not been fully developed either. There are two main mechanisms that explain this phenomenon. The first mechanism described in the early works by Parker suggests that the large-scale magnetic field is transferred by the meridional flow from the equator to the pole. In the other (the Babcock–Leighton mechanism), the tails of active regions merge with the background field and create the large-scale surface field, which moves to the pole leading to the polarity reversal of the polar field.

So far, it has not been fully verified whether either of these mechanisms is able to account for all particularities of the global magnetic field described above, as well as for its relationship with the observed effects of strong magnetic fields in the surface layers.

Acknowledgements

In this article, I have presented many results obtained in co-authorship with my colleagues A.F. Kharshiladze, B.D. Sheltig, O.G. Badalyan, E.V. Ivanova, and I.M. Liv-

shits, to whom I express my deep gratitude. The work has been supported by RSF grant No.21-72-20067.

References

Babcock H. W., Babcock H. D. (1955) ApJ 121, 349
Badalyan O. G., Obridko V. N. (2006) Sol. Phys. 238(2), 271
Badalyan O. G., Obridko V. N. (2007) AstL 33(3), 182
Brandenburg A., Rogachevskii I., Kleeorin N. (2016) NJPh 18(12), article id. 125011
Bridge H. S., Lazarus A. J., Lyon E. F., et al. (1962) J. Phys. Soc. Japan 17, Suppl. A-III, 1113
Bumba V., Howard R. (1965) ApJ 141, 1502
Bumba V., Obridko V. N. (1969) Sol. Phys. 6(1), 104
Gringauz K. I., Bezrukikh V. V., Ozerov V. D., Rybchinskii R. E. (1960) Soviet Physics: Doklady 5, 361
Gringauz K. I. (1961) Space Research II. North Holland Publishing Co. 539
Harvey J. W., Krieger A. S., Davis J. M., et al. (1975) Bull. American Astron. Soc. 7, 358
Harvey J. W., Sheeley N. R., Jr. (1977) Sol. Phys. 54, 343
Hoeksema J. T., Scherrer P. H. (1986) Solar Magnetic Field – 1976 through 1985, WCDA, Boulder, U.S.A.
Hoeksema J. T. (1991) Solar Magnetic Field – 1985 through 1990, WCDA, Boulder, U.S.A.
Howard R. (1976) ApJ. 93, L159
Ishkov V. N., Mogilevsky E. I. (1983) in: Solar Activity, Alma-Ata: Kazakh SSR Publishers, 3
Ivanov E. V., Obridko V. N., Shelting B. D. (1997) ARep 41(2), 236
Kambry M. A., Nishikawa J. (1990) Sol. Phys. 126, 89
Kane R. P. (2006) Adv. Space Res. 37, 1261
Kane R. P. (2009) Adv. Space Res. 44(10), 1252
Kleeorin N., Rogachevskii I., Ruzmaikin A. (1989) SvAL 15, 274
Kleeorin Y., Safiullin N., Kleeorin N. et al. (2016) MNRAS 460, 3960
Kovalenko V. A. (1983) Solar wind, Moscow: Nauka, 272 pp. (in Russian)
Krieger A. S., Timothy A. F., Roelof E. C. (1973) Sol. Phys. 29(2), 505
Levine R. H. (1977) ApJ 218, 291
Livshits I. M., Obridko V. N. (2006) ARep 50(11), 926
McCabe M. K., Mickey D. L., Chesley S. E. (1977) Bull. American Astron. Soc. 9, 371
Makarov V. I., Sivaraman K. R. (1989a) Sol. Phys. 119, 35
Makarov V. I., Sivaraman K. R. (1989b) Sol. Phys. 123, 367
Mogilevsky E. I. (1995) Geomagn. Aeron. 35(6), 11 (in Russian)
Mogilevsky E. I., Obridko V. N., Shilova N. S. (1997) Sol. Phys. 176(1), 107
Mogilevsky E. I., Shilova N. S. (1998) Izv. Crimean Astrophys. Obs. 94, 60 (in Russian)
Mursula K., Hiltula T. (2003) Geophys. Res. Lett. 30(22), CiteID 2135
Neugebauer M. M., Snyder C. W. (1962) Science 138, 1095

Obridko V. N. (1985) Sunspots and complexes of activity, Moscow: Nauka, 255 pp. (in Russian)
Obridko V. N. (1998) in: Feng X. H., Wei F. S., Dryer M. (eds.) Advances in Solar Connection with Transient Interplanetary Phenomena, Proc. Third SOLTIP Symp., International Academic Publishers, Beijing, 41
Obridko V. N., Shelting B. D. (1999) Sol. Phys. 184(1), 187
Obridko V. N., Shelting B. D., Kharshiladze A. F. (2006) Geomagn. Aeron. 46(3), 294
Obridko V. N., Vaisberg O. L. (2017) Solar System Res. 51(2), 165
Obridko V. N., Shelting B. D. (1987a) Geomagn. Aeron. 27, 197
Obridko V. N., Shelting B. D. (1987b) Geomagn. Aeron. 27, 660
Obridko V. N., Shelting B. D. (1988a) Kinem. Fiz. Nebesn. Tel 4, 29
Obridko V. N., Shelting B. D. (1988b) Soln. Dannye 1, 89 (in Russian)
Obridko V. N., Shelting B. D. (1989) Sol. Phys. 124, 73
Obridko V. N., Shelting B. D. (1990) AZh. 67, 890
Obridko V. N., Shelting B. D. (2000a) ARep. 44, 103
Obridko V. N., Shelting B. D. (2000b) ARep. 44, 262
Obridko V. N., Shelting B. D. (2001) Sol. Phys. 201, 1
Obridko V. N., Shelting B. D. (2016) AstL 42(9), 631
Obridko V. N., Sokoloff D.D., Shelting B.D. et al. (2020) MNRAS 492, 5582
Parker E. (1955) ApJ 121, 491
Parker E. N. (1958a) ApJ 128, 664
Parker E. N. (1958b) ApJ 128, 677
Parker E. N. (1959) J. Geophys. Res. 64, 1675
Rogachevskii I., Kleeorin N. (2007) Phys. Rev. E 76(5), id. 056307
Rozelot J. P. (1983) Ann. Phys. (Paris) 8(5–6), 539
Safiullin N., Kleeorin N., Porshnev S., et al. (2018) J. Plasma Phys. 84, id. 735840306
Schulz M. (1973) Ap&SS 24(2), 371
Sheeley N. R., Jr., Harvey J. W., Feldman W. C. (1976) Sol. Phys. 49, 271
Shibata K., Nitta N., Strong K. T., et al. (1994) ApJ 431(1), L51
Švestka Z., Olmr J. (1966) Type IV Bursts. I. List of Events. Bulletin of the Astronomical Institute of Czechoslovakia, vol. 17, p. 4
Švestka Z. (1968) On Long-Term Forecasts of Proton Flares. Solar Physics, vol. 4(1), pp. 18–29
Smith E. J., Tsurutani B. T., Rosenberg R. L. (1978) JGR 83(A2), 717
Waldmeier M. (1950) Zeitschrift f. Astrophysik 27, 24
Wang Y.-M., Hawley S. H., Sheeley N.R., Jr. (1996) Science, 271, 464
Yazev S. A. (2014) Phenomenon of the complexes of activity in the Sun, Irkutsk: IGU, 400 pp. (in Russian)
Zirin H. (1975) Bull. American Astron. Soc. 7, 359